Sidewall Boundary-Layer Removal and Wall Adaptation Studies

A. V. Murthy*
Vigyan Research Associates, Hampton, Virginia
and
E. J. Ray†
NASA Langley Research Center, Hampton, Virginia

This paper describes the NASA Langley Research Center 0.3-m Transonic Cryogenic Tunnel sidewall boundary-layer removal system and its integrated operation with the adaptive wall adjustment. Empty test-section measurements show that the sidewall boundary-layer displacement thickness at the model station is reduced from about 1.0 to 0.6% of the test section width when the maximum boundary-layer removal conditions are applied. Tests with a supercritical airfoil model show that the iterative top and bottom wall adaptation process performs satisfactorily with sidewall boundary-layer removal. The top and bottom walls move together to correct for the freestream Mach number changes associated with the boundary-layer removal. The airfoil test showed that the boundary-layer removal does not significantly influence the midspan measurements for thin sidewall boundary layers ($2\delta^*/b < 0.01$). With successful operation of iterative wall adaptation and sidewall boundary-layer removal, under cryogenic-pressure conditions, the 0.3-m Transonic Cryogenic Tunnel provides the potential for airfoil testing at flight-equivalent Reynolds numbers and low wall interference.

Nomenclature

b = test section width
c = airfoil chord
c_d = section wake drag force coefficient
c_n = section normal force coefficient
dz = wall movements
h = test section height
H = sidewall boundary-layer shape factor
L = reference length scale, 2.54 cm
M = freestream Mach number
m = mass flow rate
n = index of power law in boundary-layer velocity profile
R = unit Reynolds number, per meter
R_c = Reynolds number based on airfoil chord
X = distance along the test section from turntable center
x = distance from the airfoil leading edge
y = distance from sidewall (in boundary layer)
z = top and bottom wall vertical displacement
u = boundary-layer velocity
α = airfoil angle of attack (deg)
δ^* = boundary-layer displacement thickness
θ = boundary-layer momentum thickness

Subscripts

e = conditions at edge of boundary layer
l = local values
bl = boundary layer
ts = test section

Presented as Paper 89-0148 at the AIAA 27th Aerospace Sciences Meeting, Reno, NV, Jan. 9–12, 1989; received Feb. 16, 1989; revision received Dec. 12, 1989.

*Consultant. Member AIAA.
†Aerospace Engineer. Member AIAA.

Introduction

ADAPTIVE wall test sections are finding increased use in transonic wind-tunnel testing of airfoils.[1,2] The main advantage of adaptive walls is that they provide the potential of using larger models in a given test section with low wall interference. The purpose of the adaptive walls is to modify the flow conditions at the test-section boundaries in a systematic manner to eliminate wall interference at the model.

Two different approaches have been taken in using the adaptive wall technique. The first method, based on the original studies at the National Physical Laboratory in England,[3] uses flexible, solid, top, and bottom walls in the test section. During the test, the solid, top, and bottom walls are adjusted to the free-air streamline shapes to eliminate the wall effects on the airfoil measurements. The second method[2] uses ventilated walls with the ability to control the flow through the walls to remove wall interference effects at the model station.

The adaptive wall technique pursued in the NASA Langley Research Center 0.3-m Transonic Cryogenic Tunnel (TCT)[4,5] is based on the National Physical Laboratory concept using the solid flexible walls. The 0.3-m TCT uses the cryogenic-pressure tunnel concept to simulate flight equivalent Reynolds numbers on typical airfoil models of about 15 cm chord length. The combined adaptive wall and the cryogenic-pressure capabilities of the 0.3-m TCT affords high Reynolds number airfoil research under conditions virtually free of wall interference.

In addition to top and bottom wall interference, the boundary layers on the sidewalls of the tunnel introduce yet another kind of interference in two-dimensional testing. The sidewall boundary-layer effects are three dimensional in nature. To minimize the sidewall boundary-layer effects on the model measurements, modern airfoil testing tunnels[6] use some kind of boundary-layer removal on the test-section sidewalls. The removal of flow from the sidewalls reduces boundary-layer thickness and, hence, delays separation from the walls.

The 0.3-m TCT is equipped with a sidewall boundary-layer removal system. The removal system, now under evaluation, has two main features. First, it uses perforated suction panels with a smooth flow surface that do not thicken the boundary layer when there is no removal. Second, the removal system is designed to give adequate removal capability over the entire

operating envelope of the tunnel without upsetting the test condition equilibrium. The current removal station is upstream of the model. However, with modifications, the system can be used for boundary-layer removal at other stations around the model or at a downstream station.

This paper describes the 0.3-m TCT sidewall boundary-layer removal system and its integration with the adaptive wall process. The studies included sidewall boundary-layer measurements in the empty test section and tests on a large chord supercritical airfoil. The airfoil chord to tunnel height ratio was about 0.7. This relatively large model size combined with sidewall boundary-layer removal represents a severe test of the wall streamlining process used in the 0.3-m TCT.

Apparatus

0.3-m Transonic Cryogenic Tunnel

The 0.3-m TCT (see Fig. 1) is a continuous flow fan driven transonic tunnel using cryogenic nitrogen as the test gas. The drive motor for the fan is variable frequency with a maximum power of 2250 kW. The test Mach number range is from about 0.05 to 0.95. The stagnation pressure and temperature are variable in the range 122–608 kPa (1.2–6 atm) and 80–320 K, respectively. The liquid nitrogen injected into the tunnel circuit (see Fig. 1) cools the structure and removes the heat added to the stream by the fan. An automatically controlled gaseous nitrogen exhaust valve maintains steady operating pressures in the tunnel. A digital control system enables independent variation of test Mach number, stagnation pressure, and stagnation temperature.

Adaptive Wall Test Section

The two-dimensional adaptive wall test section (see fig. 2) has flexible top and bottom walls and rigid sidewalls. The test section width is 0.33 m. The nominal height between the top and bottom walls is also 0.33 m. The overall length of the test section is 1.86 m.

The top and bottom walls are of thin stainless steel plates suitable for operation at cryogenic temperatures. The plate thickness varies along the length. The thickness is maximum (0.95 cm) at the upstream end. Near the model region, where the wall movements are larger, the thickness is 0.16 cm. Twenty-one jacks on each wall support the flexible walls and provide the wall-shaping capability. The upstream ends of the walls are anchored whereas the downstream ends are free to move in sliding joints. The jacks that shape the walls are driven by individual stepping motors. A pressure shell encloses the test section. The push rods connecting the plates to the jacks pass through cutouts in the pressure shell. The drive system components are outside the pressure shell and are not exposed to cryogenic temperatures. A dedicated microprocessor monitors the wall movements.

Linear variable differential transducers (LVDT) at the jack stations provide the wall position data. The pressure orifices along the flexible wall centerlines at the various jack stations give the necessary pressure data. The wall adjustment strategy

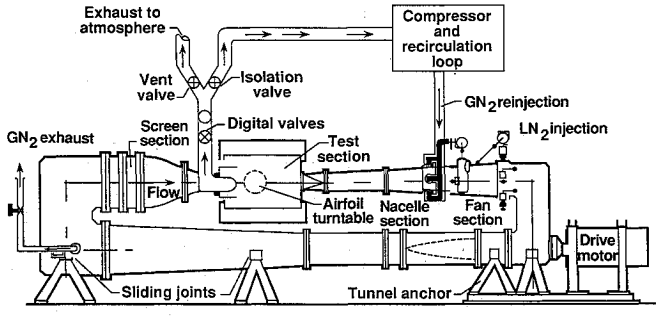

Fig. 1 Schematic of NASA Langley 0.3-m transonic cryogenic tunnel.

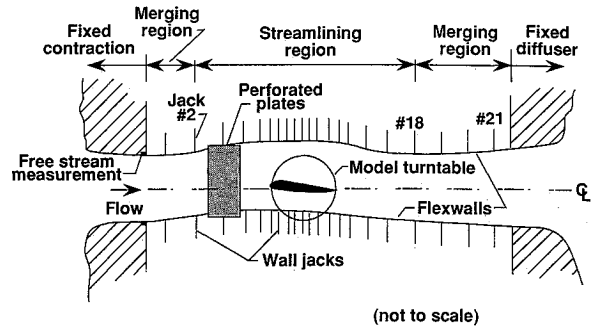

Fig. 2 Schematic of NASA Langley 0.3-m transonic cryogenic tunnel adaptive wall test section.

uses the wall position and pressure information to drive the walls to the streamline shapes during a test. The wall "streamlining" calculation uses only the data at the first 18 jack locations. The last three jack stations provide a smooth transition to the test-section exit at the beginning of the diffuser.

The airfoil models span the width of the test section and mount to circular turntables in the tunnel sidewalls. A computer-controlled stepper motor drives the turntable angle-of-attack mechanism. A sidewall-mounted drag rake traverses vertically through the airfoil wake for drag measurements. The sidewall has provision for mounting the drag rake at three different locations downstream of the turntables.

Boundary-Layer Removal System

The boundary-layer removal system has a pair of perforated panels (see Fig. 2) mounted on the tunnel sidewalls upstream of the model. The perforated panels are 0.17 m wide and 0.33 m high and extend from the tunnel floor to the ceiling. The panels have fine holes drilled by electron beam technique. The holes have a nominal diameter of 0.25 mm and are 0.75 mm apart, giving an open area of about 10%. The plate-flow surface has been made extremely smooth by etching and polishing procedures. Earlier studies[7,8] have shown the perforated panels made by this method to be superior to plates of conventional sintered materials. The boundary-layer thickening, due to surface roughness or hole openings, has been shown to be much less with electron-beam drilled perforated panels. A honeycomb structure glued to the backside supports the perforated panels.

The boundary-layer mass taken out of the test section passes through digital flow control valves (see Fig. 1). The digital valves consist of a number of calibrated sonic nozzles. These nozzles open or close in appropriate combinations to control the rate of mass removal from the test section. A dedicated microprocessor commands the operation of the nozzles.

The boundary-layer removal system operates in two modes, either passive or active. In the passive mode, the gas removed from the boundary layer exhausts directly to the atmosphere. Therefore, for this mode of operation, the test section static pressure must be higher than the ambient atmospheric pressure. Also, the maximum amount of boundary-layer mass that can be removed is directly related to the quantity of liquid nitrogen injected. This requirement is necessary to maintain equilibrium operating conditions. The amount of liquid nitrogen injected into the tunnel increases at higher Mach numbers and pressures due to larger fan-drive power requirements. Hence, instead of the normal exhaust procedure, venting nitrogen gas through boundary-layer removal offers an acceptable mode of operation.

Unlike the passive mode, the active mode was designed to work over the entire operating envelope of the tunnel. The active mode is required at low test Mach numbers and low pressures when the amount of liquid nitrogen injected is small.

In the active mode, the mass removed from the test section is injected back into the tunnel circuit to maintain equilibrium conditions. A centrifugal compressor recompresses the gas. The compressed gas is cooled before injecting into the tunnel circuit diffuser. A detailed description of the active boundary-layer removal system is given in Ref. 9.

For the present studies, the boundary-layer removal operation was in the passive mode. A maximum removal rate of about 1.6% of the test-section mass flow was available in the passive mode at a Mach number of 0.76 and Reynolds number of 87×10^6/m. It must also be realized that removing higher amounts by active operation may only introduce larger Mach number changes without significantly thinning the boundary layer at the model station. Therefore, the passive mode of operation is adequate to study the combined operation of the boundary-layer removal and the wall streamlining process.

Adaptive Wall Adjustment Strategy

The top and bottom wall adjustment strategy used in the 0.3-m TCT is based on the method of Judd et al.[10] The strategy represents the walls with vorticity panels. The difference between the measured pressures and the calculated values for the wall shape determines the vorticity strength of each panel. The difference is minimized by successive iterations, each time measuring the pressures and then moving the walls to the new position. This process eventually results in streamlining the walls to free-air streamline shapes within a specified accuracy.

The method of Ref. 10 has been automated[11] into a software process to make it easier to test airfoils in the 0.3-m TCT adaptive wall-test section. The present study used this method in the testing of a supercritical airfoil with sidewall boundary-layer removal.

The removal of the sidewall boundary layer has two effects. The boundary-layer thins downstream of the removal region. This is the desirable effect. However, the removal of the boundary layer also reduces the Mach number in a constant area test section. A simple way to account for the Mach number change is by calculating initial wall shapes assuming the sidewall boundary-layer removal effect to be one dimensional. The method of Ref. 6 uses this approach. However, the iterative adjustment process eliminates the need to precalculate the wall shapes. The pressure changes associated with sidewall boundary-layer removal are superimposed on the changes due to the airfoil. The wall adjustment process then responds to the combined effects produced by the removal of the boundary layer from the test section and the presence of the airfoil. The iterative method is advantageous over using the simple one-dimensional approach because it automatically accounts for the complicated interaction between the airfoil flowfield and the sidewall boundary layer.

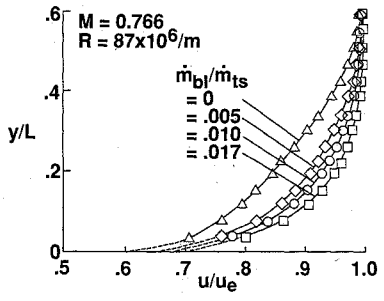

Fig. 3 Boundary-layer velocity profiles for different removal rates (empty test section).

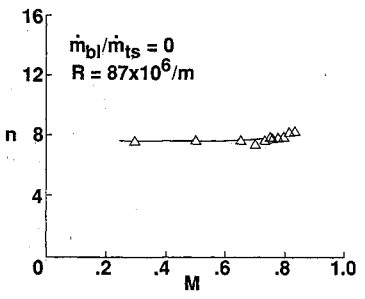

Fig. 4 Variation of index n in power law with Mach number for zero removal rate (empty test section).

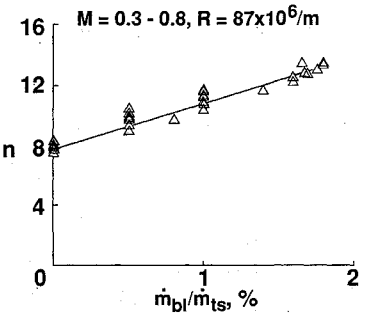

Fig. 5 Variation of index n in power law with boundary-layer removal (empty test section).

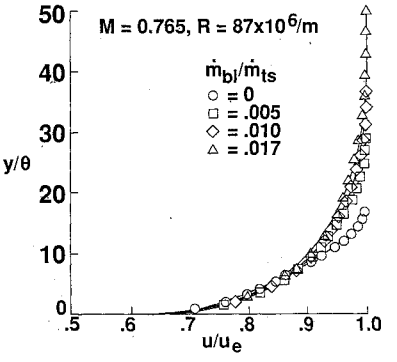

Fig. 6 Correlation of boundary-layer velocity profiles in terms of momentum thickness (empty test section).

Results and Discussion

Boundary-Layer Measurements

Empty test-section boundary-layer thickness at the model station is a measure of the extent of sidewall boundary-layer influence. Hence, before the airfoil tests, the empty test-section boundary-layer characteristics were measured using a small multitube total pressure rake. The rake was mounted on the sidewalls in the model region, about 25 cm downstream of the boundary-layer removal region. The rake had 15 total pressure tubes spaced equally 1 mm apart.

Boundary-layer rake measurements were made in the empty test section over a range of Mach numbers at a Reynolds number of 87×10^6/m. The flexible top and bottom walls were set to aerodynamically straight contours corresponding to zero removal conditions. The measured boundary-layer pressures were converted to velocities by using Crocco's relation for the temperature and velocity variation.

Figure 3 shows the typical change in the boundary-layer velocity profile at the model station for different levels of upstream boundary-layer removal at the model station. With increasing boundary-layer removal rates, from 0 to a maximum removal rate of about 1.6% of the test-section mass flow, the velocity within the boundary layer increases gradually.

Most of the measurement points in the boundary layer lie in the outer region of the turbulent boundary layer. Hence, a

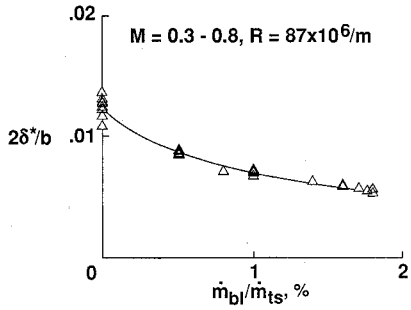

Fig. 7 Displacement thickness variation at model station with upstream boundary-layer removal (empty test section).

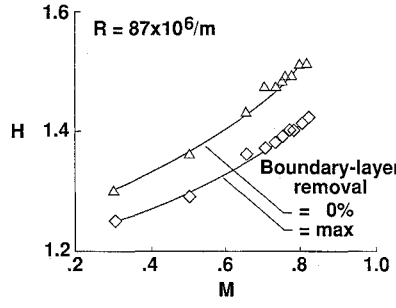

Fig. 8 Shape factor variation with upstream boundary-layer removal (empty test section).

power-law approximation was used to extrapolate the data from the wall to the first tube. The index n in the power law ($y \propto u^{1/n}$) is about 7 for all conditions with no removal in the Mach number range 0.3–0.8 (see Fig. 4). However, n was shown to be highly dependent on the boundary-layer removal rate, increasing from about 7 with no removal to about 13 with maximum removal (see Fig. 5). The measured velocity profiles for different nonzero boundary-layer removal rates show good correlation (see Fig. 6) when plotted in terms of the momentum thickness (y/θ).

The displacement thickness parameter $2\delta^*/b$ and the shape factor H are of interest in correcting airfoil test data for sidewall effects. Figure 7 shows the variation of $2\delta^*/b$ with boundary-layer removal in the Mach number range 0.3–0.8 for a freestream Reynolds number of 87×10^6/m. The parameter $2\delta^*/b$ reduces from about 0.013 without removal to 0.006 with maximum removal rate of about 1.6% of the test-section flow. The boundary-layer removal is most effective up to about 1% removal rate. This demonstrates that higher removal rates only introduce large Mach number changes without significantly improving the sidewall boundary-layer conditions.

Figure 8 shows the variation of H with Mach number for the extremes of boundary-layer removal. The variation is similar for conditions with and without sidewall boundary-layer removal. The shape factor H reduces by about 0.1 under maximum removal conditions. The dependence on Mach number is strong, increasing from about 1.25 to 1.4, for the maximum removal condition over the Mach number range.

The location of the boundary-layer removal region with respect to the model location is important. If the removal station is too far ahead, the effectiveness of boundary-layer removal is lost due to rapid growth of the boundary-layer downstream of the removal region. If the removal region is too close to the model, the boundary-layer removal may influence the flow over the airfoil. The gradual decrease in the boundary-layer thickness (see Fig. 7) at the model station suggests the present upstream, boundary-layer removal location is satisfactory.

Airfoil Tests

A long chord supercritical airfoil model was used to study the combined sidewall boundary-layer removal effect in the adaptive wall operation. The airfoil section thickness was about 12%. The model chord was 23 cm, giving a chord to test section height ratio (c/h) of 0.70. Typical test results obtained at a Mach number of 0.765 and Reynolds number of 20×10^6 are presented.

The sidewall boundary layer thins in the airfoil region due to acceleration of the flow. This effect introduces a negative blockage due to the widening of the flow passage. Hence, the airfoil lift will be correspondingly lower compared to the case without sidewall boundary layers. The reduction in lift is directly proportional to the sidewall boundary-layer displacement thickness. At higher Mach number, the widening of the flow passage also introduces a negative correction for the test Mach number. By keeping the boundary-layer thickness small by upstream removal, it is possible to keep the correction to test Mach number small.

The airfoil tests were made for conditions with and without sidewall boundary-layer removal. For both the conditions tested, the iterative wall adjustment process worked satisfactorily and converged to final wall shapes without difficulty. The number of iterations required for convergence was about the same with or without the sidewall boundary-layer removal.

Figure 9 shows the local Mach numbers on the airfoil surface and the converged top and bottom wall positions for $M = 0.765$ and $\alpha = 1.1$ deg. For this condition, the effect of sidewall, boundary-layer removal ($\dot{m}_{bl}/\dot{m}_{ts} = 0.016$) on the airfoil pressure distribution is negligible on the lower surface. On the upper surface, the shock appears to move slightly down-

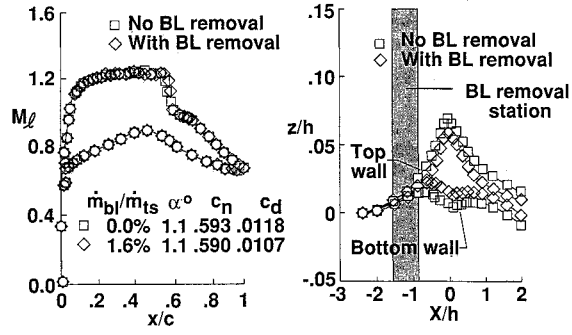

a) Local Mach number (airfoil) b) Wall shapes

Fig. 9 Effect of upstream boundary-layer removal on airfoil local Mach number and top and bottom wall shapes: $M = 0.765$, $R_c = 20 \times 10^6$, $\alpha = 1.1$ deg.

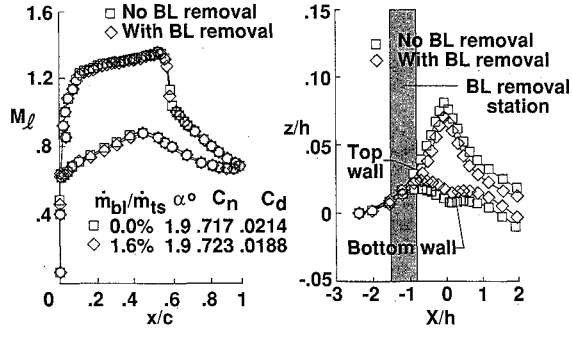

a) Local Mach number (airfoil) b) Wall shapes

Fig. 10 Effect of upstream boundary-layer removal on airfoil local Mach number and top and bottom wall shapes: $M = 0.765$, $R_c = 20 \times 10^6$, $\alpha = 1.9$ deg.

stream with boundary-layer removal. However, the change is not significant.

Although the airfoil pressure distribution did not change much, the boundary-layer removal had a strong effect on the converged wall position (see Fig. 9b). Downstream of the removal region, both the top and bottom walls moved inwards together with sidewall boundary-layer removal. This is because the removal of mass flow from the test section results in a reduction of the test Mach number downstream of the removal region. The wall adjustment strategy responds to the change and drives the walls to a position to hold the test Mach number constant in the model region.

Figure 10 shows similar effects of sidewall boundary-layer removal at a higher incidence $\alpha = 1.9$ deg where the shock is much stronger. The effect on airfoil pressure distribution is again not significant. The wall movements due to sidewall boundary-layer removal are about the same as for the 1.1-deg incidence case.

The corresponding top and bottom wall local Mach number distributions for the two angle of attack conditions are shown in Fig. 11. Since the changes in Mach number due to boundary-layer removal are compensated by corresponding wall movements, there is not a significant change in wall Mach numbers for conditions with and without boundary-layer removal. The peak Mach number on the top wall is about 0.95 for the conditions considered. On the bottom wall, the Mach numbers are slightly lower for the case with boundary-layer removal than with no removal.

Because of the relatively thin sidewall boundary-layers in the 0.3-m TCT, it appears that the boundary-layer removal affects mainly the wall positions without significantly affecting pressures on the airfoil and the top and bottom walls. Figure 12a shows the change in wall positions due to boundary-layer removal only. This parameter is obtained by subtracting the wall position with boundary-layer removal from the position without removal. The top wall movements along its length are almost identical for the different airfoil incidences. The bottom wall shows small differences that might be due to a nonuniform effect of boundary-layer removal. The total change in the combined top and bottom wall movement downstream of the removal region is shown in Fig. 12b. The measured change in wall positions is slightly higher than the one-dimensional predictions, which are proportional to the mass flow removed. As mentioned earlier, the upstream and downstream influence of the boundary-layer removal is not accounted for in the one-dimensional theory.

The comparison of the airfoil normal and drag-force characteristics is shown in Fig. 13. The angle of attack was varied from low lift to stall conditions. The comparison shows there is no significant effect of sidewall boundary-layer removal on the normal and drag force characteristics for this supercritical airfoil.

The closeness of the data between the removal and no removal conditions suggests that the midspan measurements on airfoils in the 0.3-m TCT are relatively free of contamination by sidewall boundary-layer effects. This can be due to two reasons. First, the sidewall boundary layers are relatively thin. The displacement thickness is only about 1% of the test section width. Second, the boundary-layer removal plates are smooth and do not significantly thicken the sidewall boundary layers when there is no removal. One additional possibility is that the iterative wall streamlining process partially compensates for the sidewall boundary-layer effects.

The discussions thus far have attempted to show that flight equivalent airfoil results can be obtained at near interference free conditions in the 0.3-m TCT facility. However, other uncertainties such as residual interferences may be still present in the test data from adaptive wall test sections. Therefore, a careful evaluation of the test data is necessary to determine if

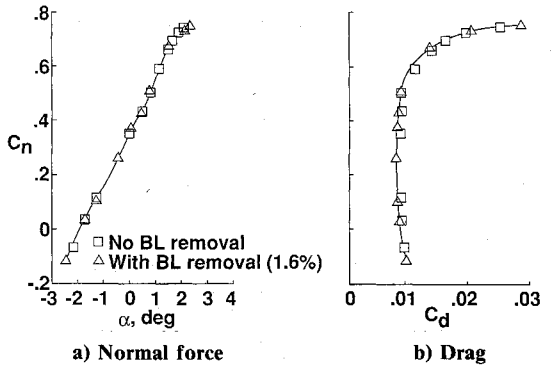

Fig. 13 Comparison of airfoil normal force and drag coefficients with and without sidewall boundary-layer removal: $M = 0.765$, $R_c = 20 \times 10^6$.

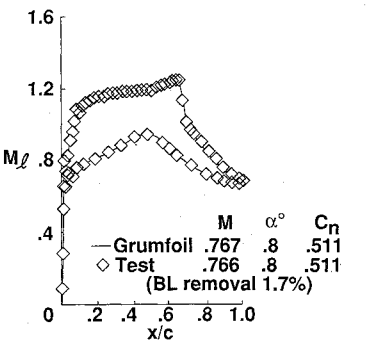

Fig. 14 Comparison of measured airfoil Mach number distribution with GRUMFOIL[12] code predictions.

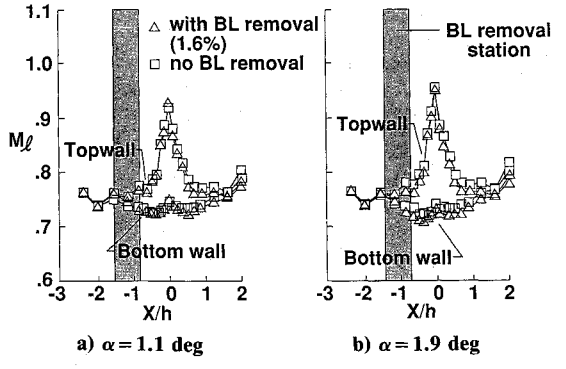

Fig. 11 Effect of boundary-layer removal on wall Mach number distribution: $M = 0.765$, $R_c = 20 \times 10^6$.

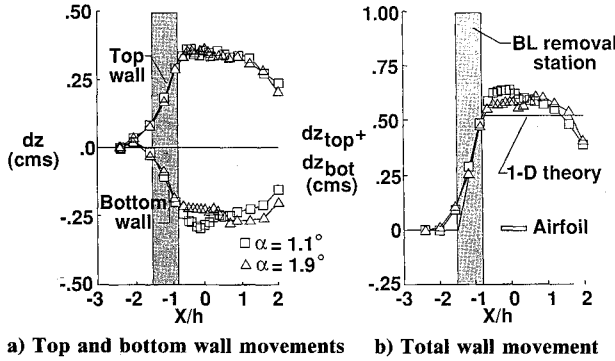

Fig. 12 Wall movements required to correct Mach number change due to boundary-layer removal.

further corrections are needed for Mach number and angle of attack.

Comparison with Theory

Figure 14 shows a favorable case of good agreement for the pressure distributions between computed results using the GRUMFOIL code[12] and the test data. The test data were taken with sidewall boundary-layer removal ($\dot{m}_{bl}/\dot{m}_{ts} = 0.017$) at a Mach number of 0.765. The sidewall boundary-layer displacement thickness was about 0.006 times the test section width (see Fig. 7). The corresponding sidewall boundary-layer correction for Mach number will be -0.004 according to Ref. 13. The top and bottom wall residual interference, calculated by a two-variable method, gives a positive Mach number correction of 0.006. These two calculated corrections nearly cancel each other, resulting in a surprisingly good agreement with the GRUMFOIL predictions.

This example illustrates that with careful testing procedures, the 0.3-m TCT adaptive wall test section can provide data with extremely low levels of wall interference. The use of the sidewall boundary removal should be considered as an additional specialty for checking selected data points suspected of significant sidewall interference. Although the observations made in this paper mainly refer to the NASA Langley 0.3-m TCT, the results are of interest to other high Reynolds number facilities with relatively thin sidewall boundary layers. Other locations on the test section sidewalls for boundary-layer removal are under consideration for the 0.3-m TCT. These locations may include boundary-layer removal around the model, in the testing of high lift devices, and downstream of the airfoil, to improve uniformity in the wake region.

Conclusions

A successful integration of a wall adaptation process with sidewall boundary-layer removal and with a large airfoil model installed in the test section has been accomplished. These unique capabilities, coupled with relatively thin boundary layers of the 0.3-m TCT, enable near interference-free testing of airfoils at flight equivalent conditions.

The studies suggest that the effects of sidewall boundary-layer removal can be small for thin boundary layers ($2\delta^*/b < 0.01$). The iterative wall adjustment method works satisfactorily with sidewall boundary-layer removal. The sidewall boundary-layer removal primarily affects the wall shapes that adapt to account for the Mach number change due to mass flow removal. For a given airfoil lift, the wall movement is less with sidewall boundary-layer removal. Hence, top and bottom wall adaptation over broader ranges of airfoil incidence and lift may be possible. A careful evaluation of airfoil data from adaptive wall test section is required to insure that residual interferences are small.

References

[1]Ganzer, U., "A Review of Adaptive Wall Wind Tunnels," *Progress in Aerospace Sciences,* Vol. 22, No. 2, 1985, pp. 81–111.

[2]Kraft, E. M., Ritter, A., and Laster, M. L., "Advances at AEDC in Treating Transonic Wind Tunnel Wall Interference," *15th ICAS Congress Proceedings,* London, England, Vol. 2, Sept. 1986, pp. 748–769.

[3]Lock, C. N. H., and Beavan, J. A., "Tunnel Interference at Compressibility Speeds Using the Flexible Walls of the Rectangular High Speed Wind Tunnel," British ARC R&M 2005, Sept. 1944.

[4]Ladson, C. L., and Ray, E. J., "Evolution, Calibration and Operational Characteristics of the Two-Dimensional Test Section of the Langley 0.3-m Transonic Cryogenic Tunnel," NASA TP-2749, Sept. 1987.

[5]Wolf, S. W. D., "Evaluation of a Flexible Wall Testing Technique to Minimize Wall Interferences in the NASA Langley 0.3-m Transonic Cryogenic Tunnel," AIAA Paper 88-0140, Jan. 1988.

[6]McDevitt, J. B., Polek, T. E., and Hand, A. L., "A New Facility for Two-Dimensional Aerodynamic Testing," *Journal of Aircraft,* Vol. 20, No. 6, 1983, pp. 543–551.

[7]Murthy, A. V., Johnson, C. B., Ray, E. J., Lawing, P. L., and Thibodeaux, J. J., "Studies of Side Wall Boundary-Layer in the Langley 0.3-Meter Transonic Cryogenic Tunnel With and Without Suction," NASA TP-2096, March 1983.

[8]Murthy, A. V., Johnson, C. B., Ray, E. J., and Stanewsky, E., "Investigation of Sidewall Boundary-Layer Removal Effects on Two Different Chord Airfoil Models in the Langley 0.3-Meter Transonic Cryogenic Tunnel," AIAA Paper 84-0598, March 1984.

[9]Johnson, C. B., Murthy, A. V., Ray, E. J., and McGhee, B. S., "Preliminary Validation of the Active Side Wall Boundary-Layer Removal System in the 0.3-Meter Transonic Cryogenic Tunnel," NASA TM-87764, Oct. 1986.

[10]Judd, M., Goodyer, M. J., and Wolf, S. W. D., "Application of the Computer for On-Site Definition and Control of Wind Tunnel Shape for Minimum Boundary Interference," *AGARD Specialists' Meeting on Numerical Methods and Windtunnel Testing,* AGARD-CP-210, Paper No. 6, Oct. 1976.

[11]Wolf, S. W. D., and Ray, E. J., "Highlights of Experience with a Flexible Walled Test Section in the NASA Langley 0.3-Meter Transonic Cryogenic Tunnel," AIAA Paper 88-2036, May 1988.

[12]Mead, H. R., and Melnik, R. E., "GRUMFOIL: A Computer Code for the Viscous Transonic Flow Over Airfoils, NASA Contractor Rept. 3806, Oct. 1985.

[13]Murthy, A. V., "Effects of Aspect Ratio and Sidewall Boundary-Layer in Airfoil Testing," *Journal of Aircraft,* Vol. 25, No. 3, 1988, pp. 244–249.